Hidden Markov Estimation of Bistatic Range From Cluttered Ultra-wideband Impulse Responses

Merrick McCracken and Neal Patwari

University of Utah, Salt Lake City, Utah, 84112, USA

***Abstract*— Multistatic radar is used for target detection and tracking in buildings and rooms. Target detection and tracking relies on accurate knowledge of the excess delay of the multipath component which travels from the transmitter, to the target, and then to the receiver. If the environment creates many multipath components, individual ultra-wideband (UWB) impulses overlap. We seek to accurately estimate a target's excess delay by considering the difference between the channel impulse response (CIR) and a known CIR of the static environment as a hidden Markov model (HMM). Experimental CIRs are used to test the performance of this model, as well as energy detection. The RMSE from applying a HMM was 2.7 ns and 2.8 ns and from applying energy detection was 5.3 ns and 5.2 ns for two experimental setups.**

I. Introduction

A useful application of ultra-wideband (UWB) impulse radios is detection and tracking of people in buildings. In particular, bistatic and multistatic radar systems are used for this application [1]. This is done by capturing the channel impulse response (CIR), $h(t)$, between pairs of radios and detecting changes to the CIR.

Assume that an UWB transmitter sends pulse $\delta(t)$. Because of multipath, the channel impulse response is described by

$$h(t) = \sum_i \alpha_i \delta(t - \tau_i), \tag{1}$$

where α_i and τ_i are the complex amplitude and time delay of the ith path, respectively. The receiver radio approximately measures the channel impulse response. Fig. 1(a) shows how the transmitted pulse follows many different paths to arrive at the receiver.

In bistatic or multistatic radar systems, the excess delay, described by $\tau_i - \tau_0$ or the difference between the arrival of a multipath and a line of sight path, is used to locate and track objects near the radio transmitters and receivers. Assuming component i is a single-bounce path (i.e. the path is affected by only one scatter as it travels from transmitter, to the target, and then to the receiver), the scatter is located on an ellipse with foci at the transmitter and receiver locations. Those scatters on multiple-bounce paths lie inside the ellipse that corresponds to τ_i. Intersecting ellipses from multiple transmitter and receiver pairs indicate possible scatter locations under a single-bounce assumption.

When a person enters the environment, the person's body will cause a new multipath component at the receiver as well as affect existing multipath components. This is illustrated in Fig. 1(b).

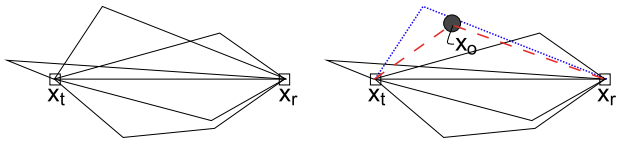

(a) Static Environment (b) Person's Effect

Fig. 1. When a person appears at x_0 in the environment between the transmitter at x_t and receiver at x_r, he causes an additional path with path length $\|x_t - x_0\| + \|x_0 - x_r\|$, and also affects multipath components with longer path lengths.

The number of multipath components seen by the receiver depends on the environment around the radios. For rooms inside of buildings, hundreds of multipath UWB pulses could be received by the receiver radio. A person may affect dozens of these paths.

This work seeks to accurately estimate τ_*, that of the path created by the person, particularly in environments with "cluttered" impulse responses, i.e., those where individual pulse delays, τ, become indistinguishable.

We consider a discrete-sampled version of the power-delay profile (PDP), r_k, where

$$r_k = \int_{(k-1/2)T}^{(k+1/2)T} |h(t)|^2 dt \tag{2}$$

where T is the sample period. In our experimental work, we use $T = 1$ ns. Essentially, r_k is the power in multipath components contained within a T-duration window near time delay kT. We call this T duration window range-bin k. The vector $\mathbf{r} = [r_1, \ldots, r_n]^T$ is the sequence of r_k samples.

Estimation of τ_* is performed by considering the changes to r_k relative to the known r_k of the static environment as a hidden Markov model (HMM). The state of the system in range-bin k, X_k, can either be 0, representing no change, or 1, meaning r_k has been affected or changed relative to a known calibration r_k.

Estimation of k_*, where $k_* = \lfloor \frac{\tau_*}{T} \rfloor$, is equivalent to estimating τ_*. Due to multipath and the person's impact on

those later-arriving multipath, r_k will experience changes, or $X_k = 1$, for many $k \geq k_*$. The advantage of applying a HMM is that X_k is considered over all k rather than considering changes at each k independently of all other k.

A. Related work

Sun et al. use a HMM to improve the performance of detecting channel use in dynamic spectrum access [2]. The authors simulated channel access by primary users and the performance of detection by secondary users, who would use the channel opportunistically, using a HMM and comparing it to energy detection. Their simulations showed improved detection performance for the HMM over energy detection.

Nijsure et al. modeled a HMM tracking system for UWB radar signals and simulated its performance [3]. This model differs from the one proposed in this work, however. In their work, the states of the model are different geographic regions near the radios rather than changes to the received signal. They assume an unambiguous power delay profile, which is the received power and time delay associated with each multipath reflection. The radios are configured in a monostatic radar configuration.

SangHyun Chang et al. approach detection by modeling a human body's scattering as a spectral multipath model and cross correlating this model with the received CIRs [4], [5]. They used a UWB radio similar to those used in this work but in a monostatic radar configuration. The human body spectral multipath model was obtained using empirically collected data from their UWB radio. They collected data of a moving human subject in an open field where there was little or no multipath propagation to validate their detection method [4]. They expanded the method to tracking a human target and tested it using additional data collected from the UWB radio [5]. The experimental data for tracking was also collected in an open field.

II. Methods

A. Data Collection

Two P220 UWB radios from Time Domain are employed in capturing r_k in two rooms in the Merrill Engineering Building at the University of Utah. One room is used as a training room while the other is used as a experiment room. Figures 2(a) and 2(b) describe the positions of the radios and where the person stands in each room.

We collect both calibration measurements and measurements which represent all measurements possible in a four UWB transceiver multistatic network when a person is standing at any of the possible grid points in the two rooms. Because we have only two UWB transceivers, we conduct these measurements as follows.

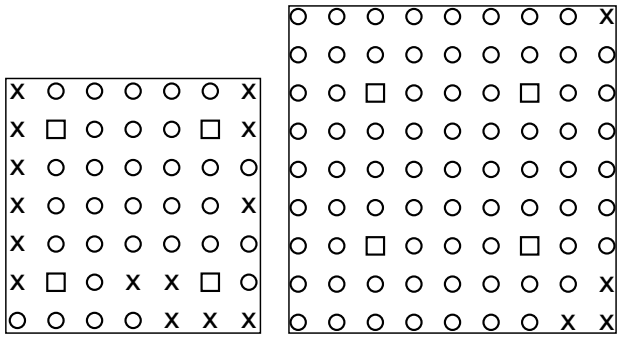

(a) Experiment Room (b) Training Room

Fig. 2. Circles are points where the person would stand, squares are radio locations, and Xs are points in the room that weren't accessible. All points are spaced 90 cm apart.

The two radios are placed in any of the four locations designated for the radios in the room. Ten calibration measurements of r_k are taken when the room is empty. Then, at each of the designated points, a person stands and remains as motionless as possible while ten more measurements of r_k are taken. This process is done for all six pair-wise radio locations in each of the two rooms.

B. CIR Changes as a Hidden Markov Model

A hidden Markov model (HMM) is a special case of a Markov chain. The states of a HMM are not directly observable but may be inferred. Other signals available for observation help determine the past and current states of the system. Let π_i be the probability of initially starting the HMM in state i, P_{ij} is the probability of transitioning from state i to state j, and $p(d_k|i)$ is the probability of observing signal d at range-bin k given the HMM is in state i. A simple illustration of a hidden Markov model is shown in Figure 3.

In the case when the observations are continuous, we use the probability density function (pdf) conditioned on the state, $p(d_k|i)$, for a continuous valued random variable. This is the typical way to describe a HMM for continuous-valued observations [6].

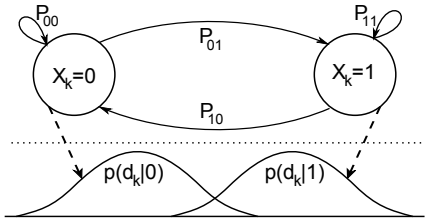

Fig. 3. The change in CIR measurement we observe at range-bin k, d_k, has a distribution dependent on the state, X_k, of a hidden Markov chain.

By knowing $p(d_k|i)$, P_{ij}, and π_i, a best estimate of the current state at each time, X_k, can be calculated. This

is found by applying the forward-backward algorithm to the sequence of observation signals. The model's transition from $X_k = 0$ to $X_{k+1} = 1$ indicates the presence of a person and allows us to estimate k_*.

A more thorough introduction to hidden Markov models and the algorithms used to infer information about them can be found in [6].

C. HMM Observations Using Kullback-Leibler Divergence

The observation signal, d_k, in this model represents the difference between r_k with a person and r_k of the empty room, that is, the calibration samples. In this work, this difference was calculated as the symmetric Kullback-Leibler (KL) divergence.

The Kullback-Leibler divergence is a measure of how many additional bits would be required to encode the samples of one distribution relative to another distribution. This is also known as relative entropy [7].

For the observed signal, d_k, we use the symmetric KL divergence assuming Gaussian distributions for r_k in both calibration and current cases. This measure is given by,

$$d_k = \frac{1}{2}\left(\frac{\sigma_p^2}{\sigma_q^2} + \frac{\sigma_q^2}{\sigma_p^2} + \frac{(\mu_p - \mu_q)^2\left(\sigma_p^2 + \sigma_q^2\right)}{\sigma_p^2\sigma_q^2}\right) - 1 \quad (3)$$

where μ_p and σ_p^2 are the mean and variance of r_k during calibration, and μ_q and σ_q^2 are the mean and variance of r_k from the current CIR measurements collected as described in Section II-A.

Other distance measures and other distributions could be applied. However, the KL-divergence and Gaussian assumption provide a standard approach for this proof-of-concept study.

D. Continuous Observation Densities

The observations d_k are continuous valued and their probability distribution is described by $p(d_k|i)$, which is the probability density function of d_k given $X_k = i$, $i \in \{0, 1\}$. The HMM parameters $p(d_k|i)$, π_i, and P_{ij} are estimated using the data collected in one room and are used as initial estimates of the HMM parameters for the other room. The data $\mathbf{d}_i$, for each state i, are made using the knowledge of k_* by

$$\mathbf{d}_0 = \{d_k | k < k_*\} \quad (4)$$

$$\mathbf{d}_1 = \{d_k | k \geq k_*\} \quad (5)$$

Dividing the observation signals in this way assumes that there will only be one transition from state 0 to state 1 and no transitions back to state 0, that is $P_{10} = 0$ and $P_{11} = 1$. This assumption is discussed further in Section II-F.

The observation densities are estimated by performing an Expectation Maximization algorithm on $\mathbf{d}_i$ to find a mixture Gaussian distribution that approximates $p(d_k|i)$. This Gaussian mixture is described by

$$p(d_k|i) = \sum_{m=1}^{M} \theta_m \mathcal{N}\left(d_k; \mu_m; \sigma_m^2\right) \quad (6)$$

where θ_m is the weight of component m, where $\sum_m \theta_m = 1$, and $\mathcal{N}\left(d_k; \mu_m; \sigma_m^2\right)$ is the Gaussian pdf with mean μ_m and variance σ_m^2 at value d_k. Initial estimates for π_i and P_{ij} are given by [6, eq. (40a-b)] using the training data.

E. HMM Solving

The HMM parameters are described by λ as

$$\lambda = [\pi_i, P_{ij}, p(d_k|i)] \quad (7)$$

The data from one room is used as training data to obtain an initial estimate of λ to begin solving for k_* with the other room's data, or that of the measurement room. The following describes how k_* is estimated for the measurement room once λ is estimated from the training data, as described previously.

Finding $\hat{X}_k$, the estimate of X_k, for the measurement room is done by solving the Forward-Backward algorithm. This algorithm finds the most likely state X at each range-bin k. After estimates for X_k are obtained, the Baum-Welch algorithm uses these estimates to update the set of HMM parameters such that

$$p(\mathbf{d}|i, \lambda_{n+1}) > p(\mathbf{d}|i, \lambda_n) \quad (8)$$

The HMM parameters are updated over all sets of $\mathbf{d}$ as described by Rabiner [6]. It is important to note that the parameters in λ are not a function of k. Also, $p(d_k|i)$ is again found by estimating the distribution as a mixture Gaussian using $\mathbf{d}_i$. However, $\mathbf{d}_i$ is now found as

$$\mathbf{d}_i = \{d_k | X_k = i\} \quad (9)$$

The algorithm continues for a set number of iterations or until the probability no longer increases more than a given tolerance with each iteration. The final estimate for k_* is

$$k_* = \min_k \{\hat{X}_k = 1\} \quad (10)$$

F. Multipath Assumptions

As τ_i increases, there are fewer multipath components. Therefore, one would expect to see fewer changes to r_k relative to the calibration r_k. However, using our model and assuming $P_{10} = 0$, the pdf of changes $p(d_k|1)$ remains constant as k increases. To improve the model, we can either a) provide a sequence of states, X_k for $k > k_*$, such that the mean of $d_k|X_k \neq 0$ reduces as a function of $k - k*$, i.e., we may have states such as $k < k_*$, $k - k_* = 0$, $k - k_* = 1$, $k - k_* = 2$, ...; or b) allow a small probability of returning from state 1 to state 0, i.e., set $P_{10} = \epsilon > 0$. In this work we chose to use method b). Future work may consider applying method a).

G. Energy detection (thresholding)

A standard method to determine the time delay caused by the target, k_*, is simply to find the first time delay at which the CIR changes by more than a threshold. We refer to this method as *first threshold crossing*. Specifically its estimate of k_* is given by

$$\hat{k}_* = \min_k d_k > \gamma \tag{11}$$

where γ is a threshold. We show the performance of this method in Figure 4 as a function of γ. To show how the method would perform with training, we assume that γ is set by using the γ that achieves the lowest RMSE in one room, and test performance with that γ in the other room.

III. Results

A. Energy Detection Results

Experiment A uses the training room and test room data as described. Experiment B swaps the data from each room and performs the experiment again. A minimum RMSE of 5.3 ns is achieved for Experiment A and 5.2 ns for Experiment B. These minimums are achieved when using the threshold that minimized RMSE for the other experiment, which served as a training threshold. Figure 4 shows how RMSE varies with the threshold.

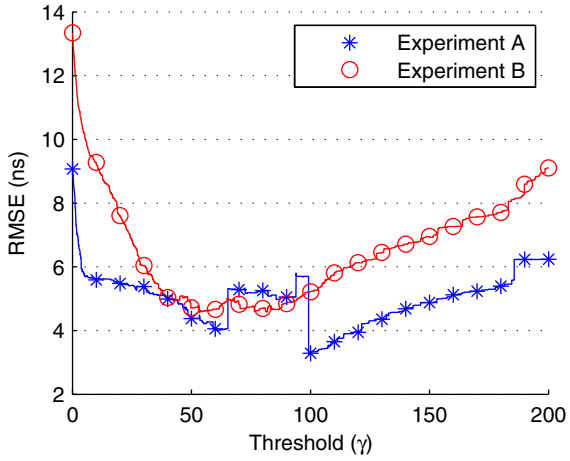

Fig. 4. Performance of *first threshold crossing* method (11) as a function of threshold γ.

B. HMM Results

The HMM and process described in Section II were applied to each room's data set to find k_* for each person location for each radio pair. The changes to RMSE for each iteration of the Baum-Welch algorithm is shown in Figure 5. The minimum RMSE achieved over 15 iterations is 2.8 ns and 2.7 ns for Experiments A and B, respectively, resulting in improvements of 47% and 48%.

The bias, $E[\hat{\tau}_* - \tau_*]$, was -0.3 ns for Experiment A and 0.2 ns for Experiment B.

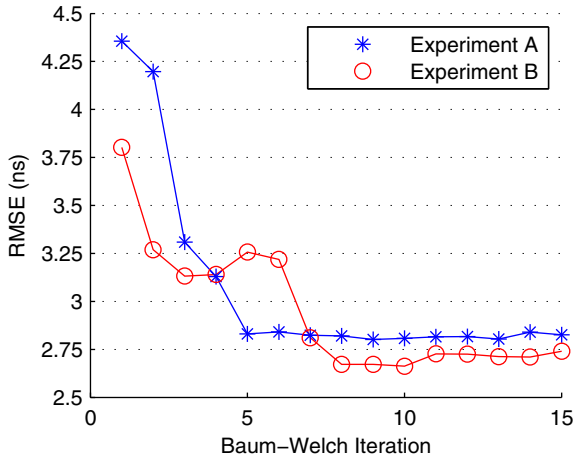

Fig. 5. Performance of HMM-based estimator of τ_* as a function of iteration count.

IV. Conclusions

Using this HMM to improve detection performance is not without limitations. This model assumes only one person is causing changes to the CIR. To account for more people, the HMM would need to include more states. Further research needs to be done to address this issue.

Experimental results show that a hidden Markov model is more effective at achieving a lower ranging RMSE than energy detection for highly cluttered multipath environments. Applying the Baum-Welch algorithm allows the estimator to achieve consistent and improved results.

Compared to using the first threshold crossing estimate of τ_*, our method reduces error by almost half. Since these estimates of excess time delay are used directly in tracking algorithms, we expect to similarly improve UWB-base localization performance.

References

[1] J. Taylor, *Ultra-wideband Radar Technology*, 1st ed. Boca Raton, FL: CRC Press, 2001.

[2] Z. Sun, G. Bradford, and J. Laneman, "Sequence Detection Algorithms for PHY-Layer Sensing in Dynamic Spectrum Access Networks," *IEEE Journal of Selected Topics in Signal Processing*, vol. 5, no. 1, pp. 97–109, Feb. 2011.

[3] Y. Nijsure, Y. Chen, C. Litchfield, and P. B. Rapajic, "Hidden Markov Model for Target Tracking With UWB Radar Systems," in *2009 IEEE 20th International Symposium on Personal, Indoor and Mobile Radio Communications*, Sept. 2009, pp. 2065–2069.

[4] S. Chang, N. Mitsumoto, and J. W. Burdick, "An algorithm for UWB radar-based human detection," in *2009 IEEE Radar Conference*, May 2009, pp. 1–6.

[5] S. Chang, M. Wolf, and J. W. Burdick, "Human Detection and Tracking via Ultra-Wideband (UWB) Radar," in *2010 IEEE International Conference on Robotics and Automation (ICRA)*, May 2010, pp. 452–457.

[6] L. Rabiner, "A Tutorial on Hidden Markov Models and Selected Applications in Speech Recognition," *Proceedings of the IEEE*, vol. 77, no. 2, pp. 257–286, Feb. 1989.

[7] T. Cover and J. Thomas, *Elements of Information Theory*, 2nd ed., ser. Wiley Series in Telecommunications and Signal Processing. Hoboken, NJ: Wiley-Interscience, 2006.